Groundwater flow modelling within a coastal alluvial plain setting using a high-resolution hydrofacies approach; Bells Creek plain, Australia

T. R. Ezzy · M. E. Cox · A. J. O'Rourke · G. J. Huftile

Abstract Ground penetrating radar (GPR) has proved to be an extremely useful geophysical tool, in conjunction with direct geological data, to develop a realistic, macroscopic, subjective-based conceptual model of aquifer architecture within a shallow coastal alluvial plain. Subsequent finite-difference groundwater modelling has not only enabled determination of the dominant groundwater flow paths for the plain, but has also quantified the effects of within-facies and between-facies sedimentary heterogeneity on those flow paths. The interconnection of narrow, unconfined alluvial channels and a broad, semi-confined alluvial delta is ensuring that most fresh groundwater that enters the plain in the form of precipitation or recharge from lateral bedrock hills, is discharged into the eastern coastal wetlands via that alluvial delta aquifer.

Résumé Le radar est un instrument géophysique très utile qui, avec les données géologiques permet les réalisations d'un modèle réaliste de la structure des aquifères alluviales côtières peu profondes. A part de la mise en évidence des directions principales d'écoulement, la modélisation par la méthode des différences finies, a permis aussi de quantifier les effets des hétérogénéités des faciès sédimentaires au long des mêmes directions d'écoulement. L'interconnectivité des canaux alluviaux libres avec une delta semi captive assure que la plupart de l'eau douce de la plaine provenant de précipitations or par la recharge du substratum qui affleure dans les collines latérales se décharge dans les marécages côtières á travers de l'aquifère deltaïque.

Resumen El radar de penetración terrestre (RPT), ha demostrado ser una herramienta geofísica de extremada utilidad, en conjunto con datos geológicos directos, para desarrollar un modelo conceptual de bases subjetivas, macroscópico y práctico, de la arquitectura del acuífero dentro de una llanura aluvial costera somera. La etapa subsiguiente del modelamiento, por diferencias finitas del agua subterránea, no solamente ha facilitado la determinación de las redes de flujo principales del agua subterránea para la llanura, si no también cuantificó los efectos de la heterogeneidad sedimentaria en la red de flujo, denominados de "facies interna" y "entre facies". La interconexión entre canales aluviales estrechos de tipo libre y el delta aluvial amplio de tipo semiconfinado, está asegurando que mucha del agua subterránea dulce que entra a la llanura, bien sea como precipitación, o bien como recarga lateral desde las colinas rocosas de los alrededores, sea descargada a los humedales costeros orientales por medio del acuífero deltaico aluvial.

Keywords Groundwater flow · Heterogeneity · Geophysical methods · Numerical modelling

Received: 21 March 2005 / Accepted: 19 May 2005
Published online: 17 March 2006

T. R. Ezzy (✉) · M. E. Cox · A. J. O'Rourke · G. J. Huftile
School of Natural Resource Sciences,
Queensland University of Technology,
GPO Box 2434, Brisbane, Queensland 4001, Australia
e-mail: tim_ezzy@urscorp.com
Tel.: +61-7-32342124
Fax: +61-7-32342199

Introduction

Sediment heterogeneity within Quaternary aquifers strongly influences spatial variability of hydraulic conductivity and the paths and rates of groundwater flow (Sudicky 1986; Anderson 1989; Woodbury and Sudicky 1991; Fogg et al. 1998; Webb and Davis 1998; Anderson et al. 1999; Klingbeil et al. 1999; Heinz et al. 2003). Heterogeneity can be considered over a wide range of scales from megascopic, defined at the scale of a well field, through to microscopic, which is present at the scale of individual grains and pores (Galloway and Sharp 1998a; Huggenberger and Aigner 1999). Macroscopic heterogeneity reflects depositional facies features such as sediment stratification, aquifer geometry and zones of internal grain size variability (both within-facies and between-facies); this intermediate scale of heterogeneity strongly influences regional and local groundwater flow systems (Dominic et al. 1998; Galloway and Sharp 1998a; Stanford and Ashley 1998; Bersezio et al. 1999).

Coastal plain settings not only contain lateral variations in facies-controlled permeability, but also unconfined, semi-confined and confined aquifers in close vertical proximity,

 DOI 10.1007/s10040-005-0470-5

reflecting complex physical stratigraphy controlled by the history of coastal evolution (Galloway and Sharp 1998b). For this reason, subjective-based conceptual models of coastal plain aquifers (that are well constrained by abundant conditioning data) are often better suited than either mathematical or process-orientated models (see Koltermann and Gorelick 1996; Carle et al. 1998; Webb and Davis 1998; Miller et al. 2000).

For subjective-based interpretations of aquifer architecture to be realistic, geophysical methods are important as they provide subsurface information linking the direct measurements made at drill holes and outcrops. The utility of particular geophysical techniques is strongly dependent on geological setting (e.g. clay- or sand-prone), the depth of data required, and the chemical character of the groundwater. Ground penetrating radar (GPR) is a high frequency electromagnetic technique that has been used to image gross aquifer geometries as well as internal sediment heterogeneities. GPR has displayed potential in a number of shallow (typically less than 20 m depth) continental and coastal sedimentary aquifer environments (Asprion and Aigner 1997; Grant et al. 1998; van Overmeeren 1998) with characteristic reflection patterns identified for sand dunes (Harari 1996; Bristow et al. 2000; Neal and Roberts 2000; Best et al. 2003), cheniers (Neal et al. 2002), lacustrine deposits (van Overmeeren 1998), Holocene floodplains (Leclerc and Hickin 1997; Nobes et al. 2001), and glacio-fluvial sediments (Bridge et al. 1995; Bridge et al. 1998; Asprion and Aigner 1999; Beres et al. 1999; Vandenberghe and van Overmeeren 1999).

In this current investigation, high-resolution GPR data is combined with direct geological observations to construct a subjective-based, conceptual model of shallow aquifer architecture within a coastal alluvial plain. Numerical groundwater flow modelling (aided by automated inverse parameter estimation) is then applied to assess the effects that sedimentary heterogeneity, both within-and between-facies, has on groundwater flow paths and rates.

Setting

Location and climate

The Bells Creek plain is situated 65 km north of Brisbane (Fig. 1b), along the eastern coast of Australia (Fig. 1a). The plain is adjacent to the northern tidal entrance of Pumicestone Passage estuary, which is protected from direct ocean swells by an elongate barrier island (Bribie Island). The area is located in a subtropical region and typically experiences hot, wet summers and cool, drier winters, although recent El Nino conditions since 2000 have resulted in dry summer months. The study site is approximately 100 km^2 in area, and is predominantly flat-lying. The coastal plain to the east is generally less than 5 m above sea level (ASL), the central alluvial plain is less than 20 mASL, and the gently undulating bedrock hills to the west reach a maximum elevation of 55 mASL. Surface runoff from the plain drains into Pumicestone Passage estuary via Lamerough, Bells and Halls Creeks (Fig. 1c). These creeks are tidal in their eastern reaches and ephemeral in the (freshwater) central and western reaches. Pine plantations are the major land use in the western and central regions, while estuarine wetlands consisting of mud flats, salt marshes, mangroves and sea grass beds are dominant to the east. Remnant patches of native *Melaleuca quinquenervia* and *Eucalyptus pilularis* occur within randomly located freshwater swamps.

Geology

The Jurassic age bedrock formation (Landsborough Sandstone) crops out in the west and north of the plain which are major recharge zones; these sedimentary sequences were deposited as thick fluviatile and swampy sheets within the Nambour Basin (Willmott and Stevens 1988; McKellar 1993). The formation has a total thickness greater than 450 m (Cranfield 1984), and contains a thick laterite weathering profile in its upper 10 to 20 m. This laterite profile typically comprises a basal saprolite layer, an extensive kaolinite-rich, mixed clay layer, as well as ferricrete layers (Ezzy et al. 2002).

From the 1960s land use practices such as forestry, agriculture, and residential development have disturbed the surface of the plain, masking the distribution of Quaternary sediments as well as the morphology of previous drainage systems. Analysis of aerial photographs taken in 1958 (preland use alterations) supplemented with drill logs of 30 preexisting hand auger borings (Martin et al. 1978) helped to reconstruct the relative distributions of major Quaternary sediments. This preliminary analysis also revealed that the central plain features alluvial channels that have incised into the laterite. Onlapping coastal deposits dominate the eastern plain in the form of beach ridges, tidal bars, estuarine swamps and low-energy beaches (Ezzy, O'Rourke, Cox, unpublished data 2003).

Materials and methods

Field data

Due to the variability of geological units within the plain, numerous drilling techniques were applied. Mud rotary and drop hammer methods were used for unconsolidated sediments and clay-rich laterite horizons, while bedrock was sampled using both diamond-tip rotary, and percussion air-hammer techniques. Within extensive clay horizons, 3 m lengths of core were obtained using hydraulic push coring. In total, 21 holes were drilled, with a permanent polyvinyl chloride (PVC) monitoring piezometer installed into each hole. Gravel pack filters were emplaced directly around the screen interval, while bentonite grout was used to seal the remainder of the hole.

Core samples and drill cuttings were individually collected at 25 cm intervals for laboratory determination of grain size, mineralogy, and degree of sorting. Visual grain size analysis was calibrated with wet and dry sieving.

 DOI 10.1007/s10040-005-0470-5

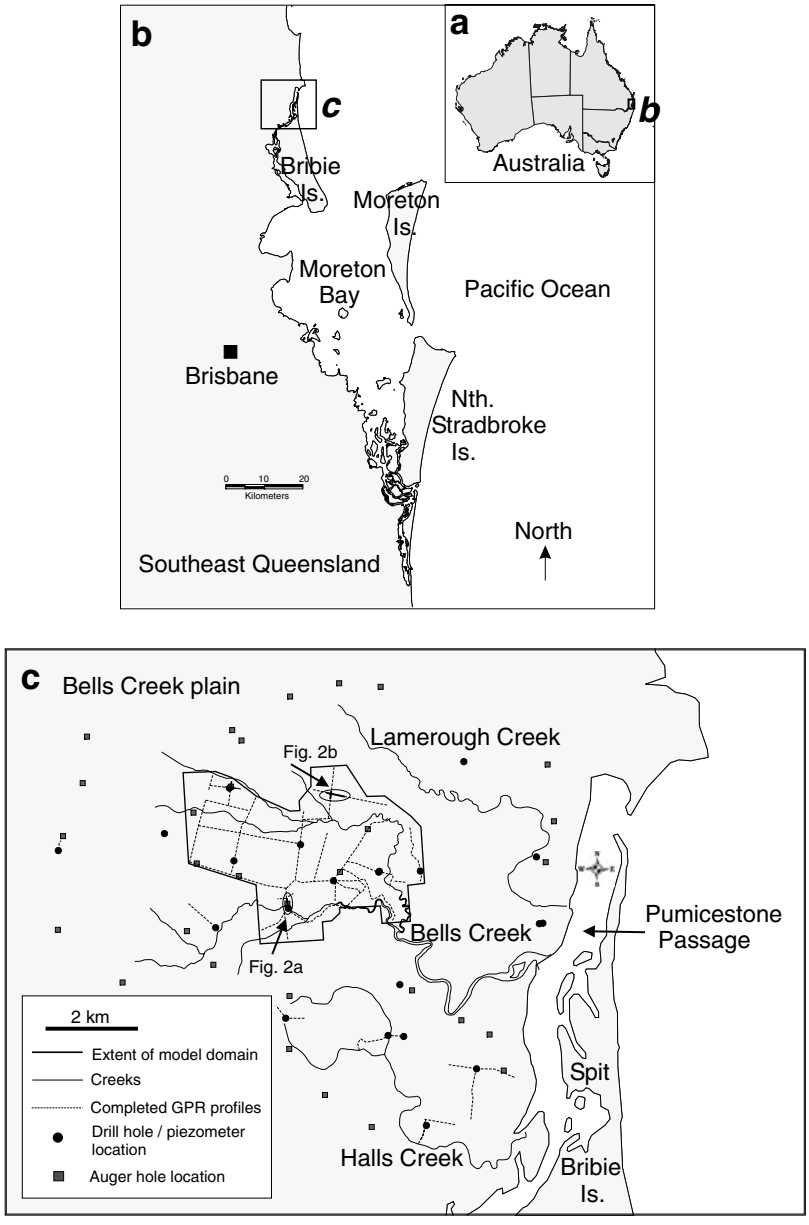

Fig. 1 Location of the Bells Creek plain, in relation to: **a** eastern coast of Australia; **b** southeast Queensland; and**c** Pumicestone Passage estuary. Fig. 1c also shows the locations of piezometers, drill and auger holes, GPR profiles, the model domain, and the drainage system

A Mala Geoscience RAMAC GPR unit with 100 Mhz antennae was used to acquire data along selected profiles over a 4-week period. Data points were triggered at a constant spacing of 0.5 m by a cotton odometer wheel connected to the control unit. Standard Mala Geoscience (RAMAC Groundvision 1.3.1) software was used to gather and process data. GPS points were collected at the start and end of every profile and at significant landmarks in between. The length of profiles varied from hundreds of meters to several kilometers, with a cumulative total exceeding 50 km (O'Rourke 2002; Ezzy, unpublished data, 2003).

Daily rainfall calculations throughout the monitoring period were based on a synthesis of regional data from nearby Bureau of Meteorology Stations, as well as on-site readings obtained from Nylex 1000 rain gauges (monitored daily at 9am by landowner).

Standing water levels were measured with an electronic dipmeter on a monthly to weekly basis, dependant upon the frequency and intensity of wet and dry events throughout the monitoring period February 2002 to February 2003.

Representative wells for each aquifer or aquitard type (alluvium, laterite clays, ferricrete horizons and floodplain clays), were subjected to pumping tests or slug tests to obtain initial estimates of hydraulic parameters (e.g. hydraulic conductivity and storativity). Drawdown and recovery data acquired from observation wells or from inside the pumping well, were analysed using AquiferTest 3.02 by Waterloo Hydrogeologic. For pumping tests on unconfined alluvial aquifer wells, both Neuman (1972) analysis and Theis (1935) analysis was used for drawdown data, and Theis analysis was used on the recovery data in those same pumping tests. The Theis (1935) method and Cooper and Jacob (1946) methods were used independently to as-

 DOI 10.1007/s10040-005-0470-5

sess drawdown in the confined basal gravel aquifer, and the Theis analysis recovery method was used for the recovery data in the gravel aquifer. For slug tests on the lower permeability units, the Bouwer and Rice method was used for analysing unconfined units and the Cooper et al. (1967) and Hvorslev (1951) methods were used for confined units.

Groundwater flow modelling

The numerical groundwater flow model was constructed using PMWin 5.0 (Chiang and Kinzelbach 1998), a graphical interface for the three-dimensional, block-centered, finite-difference code MODFLOW (McDonald and Harbaugh 1988). Both MODFLOW and MODPATH (Pollock 1989) were used to simulate groundwater flow within the selected model domain situated in the central alluvial plain.

The flow model was calibrated for a transient model run by qualitatively (pattern-matching) and quantitatively (statistical) matching predicted heads to observed heads taken in the field from February 2002 to February 2003. The calibration process incorporated several strategies to reduce the non-uniqueness problem: (a) manual trial-and-error adjustment of parameters within both measured field ranges and accepted literature ranges; (b) ensuring that multiple distinct hydrological conditions are adhered to with a particular parameter set (Middlemis 2001); (c) conducting preliminary sensitivity analysis to determine the uncertainty involved in the ranges of estimated parameters; and (d) using the nonlinear least-squares inverse model PEST (Doherty 1994) to determine the best fit parameter values.

Following calibration, a more detailed sensitivity analysis was conducted to determine the range of uncertainty involved in key hydraulic parameters within each aquifer and aquitard zone. Multipliers of 0.01, 0.1, 0.5, 0.8, 1.2, 1.5, 2.0, 5.0, 10.0, and 100.0 were applied to horizontal hydraulic conductivity ($K_h = K_x + K_y$), vertical hydraulic conductivity ($K_v = K_z$), and specific yield independently. Those three parameters were deemed to be the most sensitive in the preliminary analysis. Head values from single or paired observation wells within particular zones of interest were used to assess the uncertainty. Visual assessment (predicted versus observed heads) as well as statistical analysis were used in tandom. Statistical indices used included the slope and intercept of a least squares regression between the predicted and observed heads, the systematic and unsystematic root mean squared error (RMSEs and RMSEu, respectively), the total root mean squared error (RMSE), and an index of agreement (IOA) (see Willmott 1981 for formulae and details). The type of sensitivity (Types I to IV) of each parameter within each aquifer/aquitard was also assessed according to ASTM Standards (D 5611-94).

Results

Sedimentary facies distribution

Composite 1:12,500 aerial photographs taken in 1958 (pre-forestry practices) indicate that alluvium trends broadly west-east, in a complex network of thin channels that are approximately 50 to 400 m wide and several kilometers in length. Over 30 north-south and east-west GPR profiles revealed that those channels are typically 5 to 9 m thick, with widths of between 50 and 200 m, comparing favourably with aerial photograph interpretations (O'Rourke 2002; Ezzy, unpublished data, 2003). The channels contain relatively continuous, undulating to chaotic, variably dipping radar reflection patterns that tend to onlap onto weathered bedrock reflectors (Fig. 2a and b). Basal erosion surfaces were also common features in alluvial reflection profiles. Drilling has shown that the channels are composed of fine-grained sand in the upper 4–5 m, which grades to coarse-grained sand towards the base.

In the east of the plain, buried beneath 5–6 m of floodplain clay, the network of thin alluvial channels merge into a broad alluvial delta composed of coarse sand and gravel.

Mixed clay layers within the laterite were often limited to 1 to 2 m of radar penetration (due to rapid attenuation of the signal), and the corresponding reflection character was typically flat-lying. Elsewhere within the laterite, ferricrete horizons consisting of iron-cemented, very poorly sorted sand and gravel typically displayed up to 5 m of penetration and reflection patterns were moderately inclined, discontinuous and chaotic.

The contrasts in radar penetration and characteristic reflection patterns between the laterite and the distinctive sand-prone alluvial channels, has enabled a high-resolution isopach map of alluvial aquifer thicknesses and interconnectivity to be developed (Fig. 3).

Hydrogeological framework

Aquifer characteristics

The major aquifer within the Quaternary plain is the unconsolidated alluvium. Groundwater within the alluvium is vertically separated from sandstone bedrock groundwater by thick layers of low-permeability laterite clays (mainly kaolinite and smectite), although sandstone outcrops to the west are laterally adjacent to the landward extents of some alluvial channels. The main aquitards consist of the lateritic profile (excluding coarser ferricrete layers which host and transmit appreciable quantities of groundwater) and various clay-rich Quaternary units including estuarine, floodplain and swamp deposits.

Alluvial aquifers are unconfined in the western hills and central plain regions, and semi-confined (leaky) towards the east, where they are overlain by Holocene coastal units, and Late Pleistocene clays. The sand-rich alluvial aquifers are directly recharged by rainfall due to their surface exposure in many places. Groundwater flowpaths through the plain generally trend west-east towards the coastline, except for saline waters that permeate landward from the estuarine shoreline.

 DOI 10.1007/s10040-005-0470-5

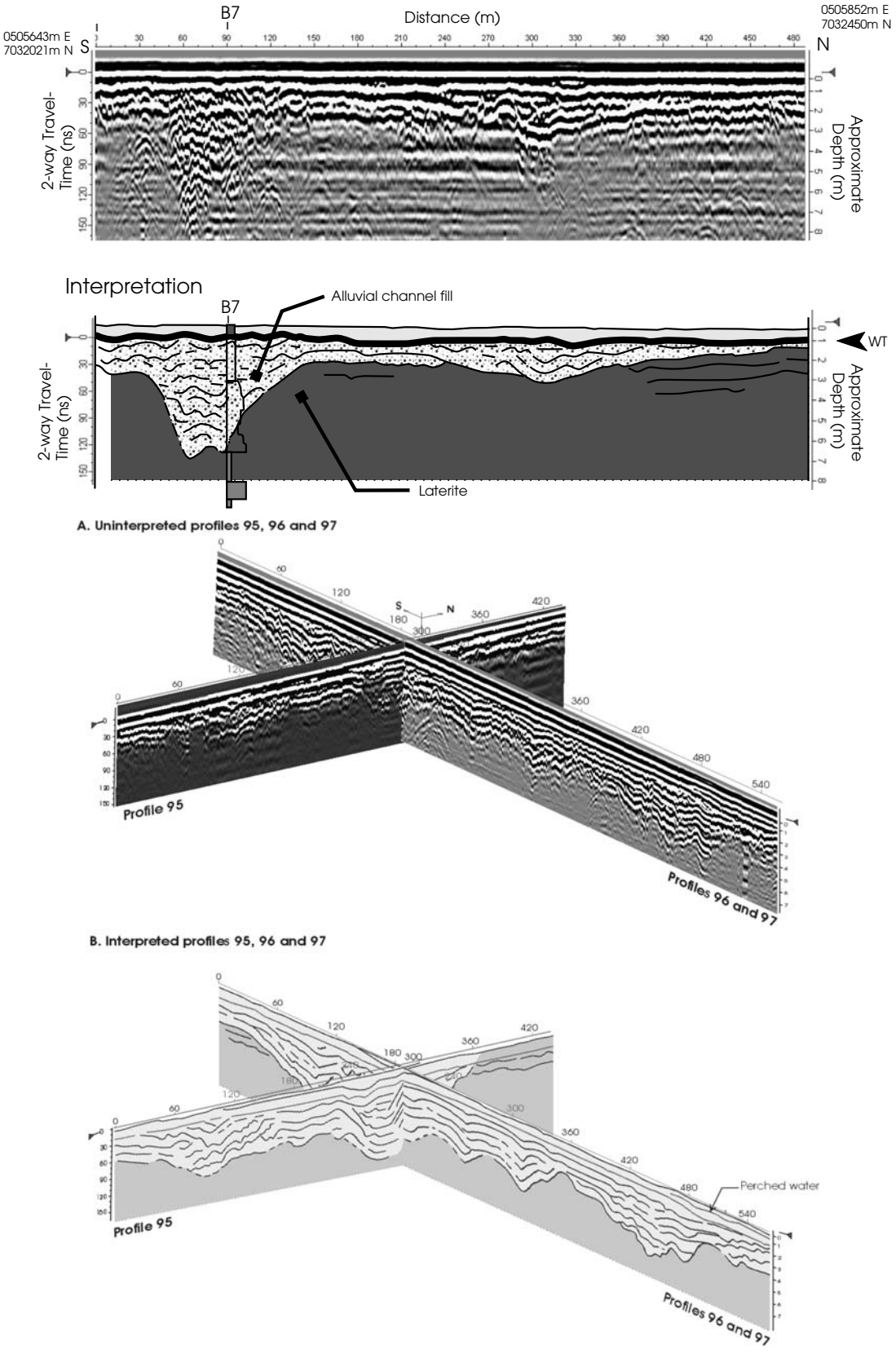

Fig. 2 **a** GPR profile and radar stratigraphic interpretation of characteristic alluvial channel environments as cross-sections and fence diagrams (profiles are located in Fig. 1c) 100 Mhz GPR profile, 500 m in length, with drill hole B7 (Fig. 3) located at 90 m. The radar stratigraphic interpretation correlates well with drill hole data, which shows channel sands to a depth of 7 m. **b** Fence diagram of 100 MHz profiles which illustrates the high level of connectivity along the sand-rich alluvial channels. Profiles 96 and 97 trend parallel to a channel axis, while profile 95 trends perpendicular across the same channel

 DOI 10.1007/s10040-005-0470-5

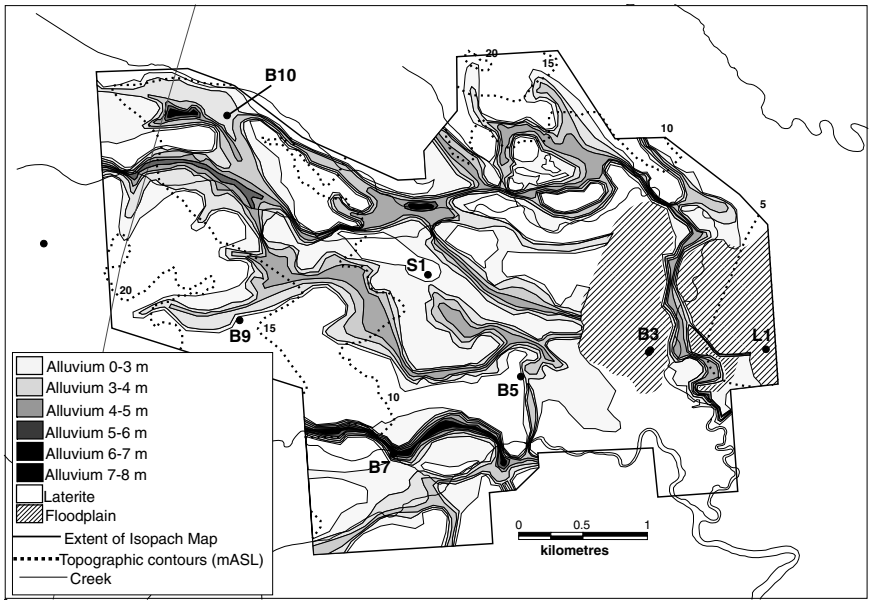

Fig. 3 Isopach map of alluvial channel thicknesses based on a synthesis of 35 km of GPR profiles. The locations of important drill holes and topography are also shown for reference, as is the location of Bells Creek

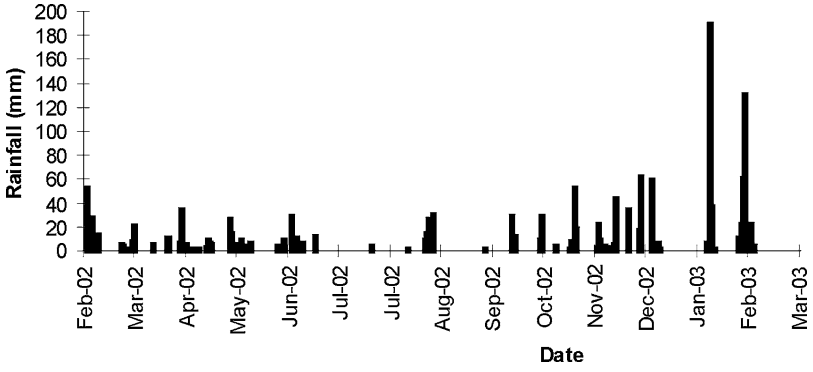

Fig. 4 Daily precipitation measurements for the Bells Creek plain based on an average of regional and local readings taken at 9.00 am daily

Rainfall patterns

From February to November 2002, it was particularly dry throughout the region, with 684 mm of rain recorded on the plain over a 10-month period at an average of 2.32 mm/day (Fig. 4). This period recorded a maximum daily event of 53 mm, and only 2 rain events over 40 mm. From December 2002 to February 2003, summer rains returned and in a 3-month period there was 763.6 mm of rain at an average of 8.49 mm/day. This period recorded a maximum daily event of 190 mm, with an additional 7 daily events over 40 mm.

Water table behaviour

The transition zone to the water table was identified clearly in GPR profiles throughout the site at a very shallow depth, typically 0 to 2 m below the surface. Piezometer measurements of standing water levels at time of acquisition (late June 2002) confirmed those shallow levels, and typically indicated a discrepancy of less than 0.4 m between the transition zone and the water table.

Trends in standing water levels, obtained from potentiometric head measurements from February 2002 to February 2003, indicate large variability in recharge and infiltration rates within the major aquifers and aquitards. Hydrographs within laterite clay wells display sharp rising limbs of between 1–2 m following significant rain events (within 1–2 weeks) usually returning to initial levels within 30 days. In areas that contained weathered bedrock at the surface, there was commonly a raised and offset water table reflector imaged by GPR. This indicates the presence of perched water bodies, due to slow infiltration rates through the kaolinite-rich clays. However, the overall trends in those hydrographs are of a 1–2 m decline associated with limited rainfall throughout the year.

Hydrograph trends from alluvial piezometers are more stable, with slight rises of 3–10 cm directly following rainfall periods. Overall, the trends have remained steady, suggesting that there is limited leakage from the groundwater within alluvium into the underlying low-permeability laterite. Notably, all of the alluvial hydrographs showed strong correlation with nearly identical trends; these observations indicate they are responding to both recharge and dry periods uniformly and that lateral connectivity between the alluvial water bodies is extremely high.

 DOI 10.1007/s10040-005-0470-5

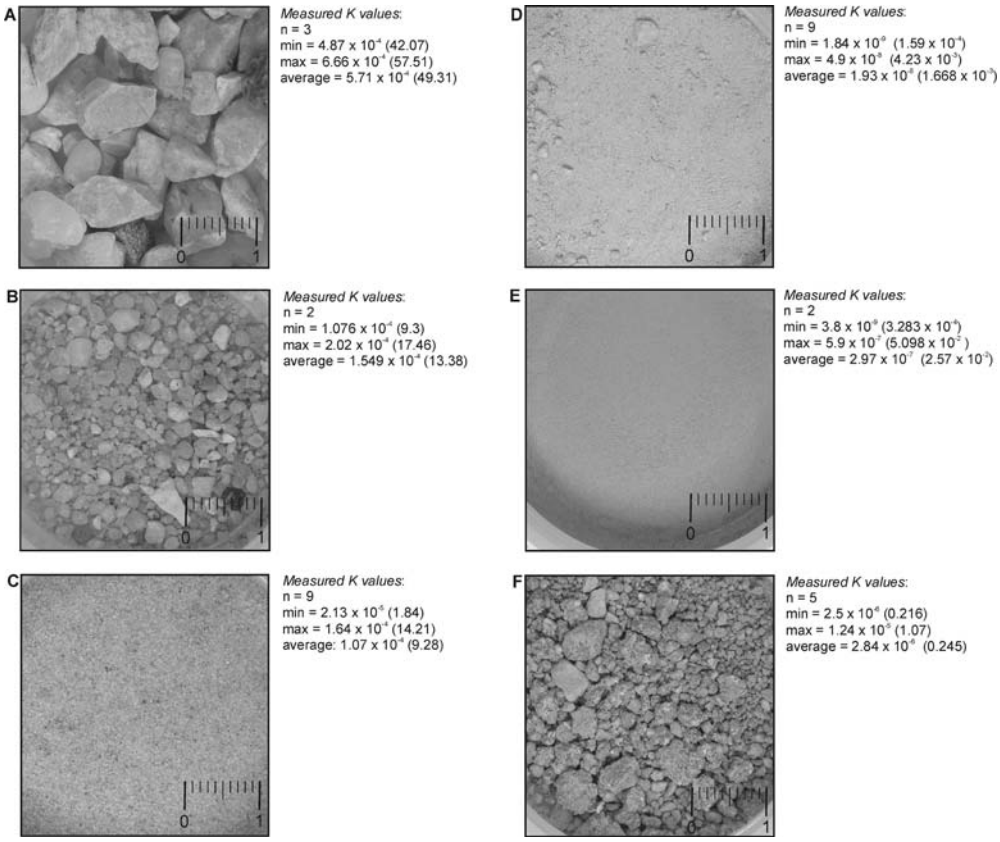

Fig. 5 Digital photographs of typical grain size and texture for each of the six hydrofacies units (labelled A to F). **A** semi-confined alluvial delta gravel; **B** medium- to coarse-grained alluvial sand (channel); **C** very fine- to fine-grained alluvial sand (channel); **D** mixed clay layer (laterite); **E** floodplain clay; **F** ferricrete horizon (laterite). Scale represents 1 cm. Measured K values for each hydrofacies unit are also given for reference. Values for K are given in m.s.$^{-1}$, with m.d.$^{-1}$ also provided in brackets for reference

Hydrofacies units and their hydraulic parameters

Hydrofacies units have been defined as interconnected sediment bodies with relatively similar hydraulic properties which determine flow paths in aquifers and control channeling of contaminants (Poeter and Gaylord 1990; Anderson et al. 1999). Six hydrofacies units (A to F) have been identified within the central Bells Creek plain, based on grain size analysis and comparison of K values obtained from aquifer pumping tests, slug tests and laboratory measurements. Figure 5 illustrates the typical grain size characteristics for each of the hydrofacies, and lists the corresponding measured K values for comparison. Unit A represents the semi-confined alluvial delta gravel in the east of the plain. The thin alluvial channels have been separated into two hydrofacies units to test the effects of internal macroscale heterogeneity on groundwater flow paths; unit B comprises medium- to coarse-grained alluvial sand at the base of the channels, and unit C consists of very fine- to fine-grained sand in the upper 4–5 m of the profile. In 9 of 13 auger and drill holes into the alluvial channels, unit C was found to also contain thin bands of organic material and illuviated clay. Units D and E have very low flow capacity and are potential flow barriers; unit D represents the mixed clay layers within the laterite, and unit E representing Pleistocene floodplain clays (which overlie unit A). Unit F represents the indurated ferricrete horizon.

Model design

The aquifer system is here represented as a two layer rectangular grid of 100 columns and 80 rows, with each cell measuring 50×50 m. The selection of cell dimensions was based on the principle of parsimony advocated by Anderson and Woessner (1992), with a trade-off between: a) the need for model simplification; b) the high resolution of the macro-scale facies model which provides detailed aquifer geometries; and c) the need for a larger number of cells (in the order of 50 or more) in zones of contrasting transmissivities, to achieve accurate flow fields (Haitjema et al. 2001). The longitudinal axis of the grid was aligned west-east, to be oriented with the general groundwater flow path within the alluvial channels. Ground surface elevations were based on DEM data (Fig. 6). The vertical thickness of layer one (unconfined) was set at 5 m, while layer two (confined/unconfined) was set at 4 m. Because the alluvial delta aquifer is only 4 to 5 m thick and is overlain by a floodplain clay unit of 5 m thickness, the layering of the model is compliant with the hydrostratigraphy. The total vertical thickness of 9 m also ensures that the maximum depth of the alluvial channels is accommodated, while enabling hydrofacies separation between the upper, very fine (unit C) and lower, coarser-grained (unit B) alluvium in the channels. Each of the six hydrofacies units (A to F) are represented as zones within the model grid (Fig. 6b and

 DOI 10.1007/s10040-005-0470-5

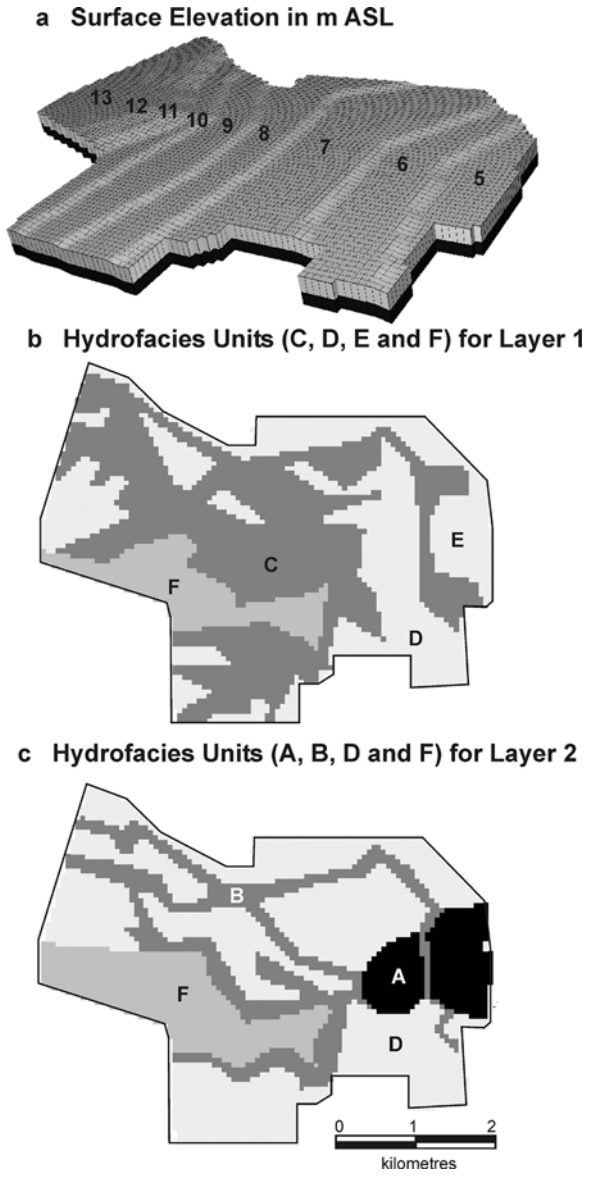

Fig. 6 Physical features of the numerical model domain: **a** a three-dimensional perspective of the model domain, showing the relief of the low-lying plain. Elevations provided are in metres ASL, and the image is vertically exaggerated by 25:1; **b** distribution of discretized hydrofacies units within layer 1 of the model domain, and; **c** distribution of discretized hydrofacies units within layer 2 of the model domain

c). Isopach maps were used to develop these zones. Layer one contains hydrofacies units C, D, E and F, and layer two contains units A, B, D and F. The bottom of the model and the lateral boundaries (to the north and south) constitute no flow boundaries.

Groundwater chemistry and hydrograph trends (Ezzy and Cox 2003) indicate that the western boundary of the model is physically adjacent to, and hydrologically connected to outcropping sandstone hills. A constant head or Dirichlet (Type 1) boundary was applied to this western boundary of the flow system. The down-gradient boundary of the flow system to the east is connected to a freshwater wetland, and in accordance with hydrograph trends is also considered as a constant head boundary. According to long-term water quality monitoring of both surface water creeks, wetlands and piezometers, the tidal influence of the Pumicestone Passage estuary does not extend into the model domain or adjacent wetlands, and for this reason variable density issues in the model are not encountered.

Recharge was assigned to the uppermost active cells, and in total 20 wet and 20 dry periods (of variable length and intensity) were applied in a transient 1-year model run. To account for high ET rates associated with forestry plots, and mixed infiltration rates of alluvium and laterite clays, recharge was initially set at 15% of precipitation for alluvium and 6% for laterite.

Initial hydraulic heads were based on output of a preliminary steady state run of dry conditions. These initial heads were compared with continuous head measurements obtained from GPR profiles, therefore providing a water table measurement every 0.5 m spacing, thus providing 100 000 head measurements throughout the model domain. Furthermore, initial heads were compared against 18 months of groundwater level measurements in fourteen additional piezometers situated throughout the entire plain. Unsaturated flow is not accounted for in this model.

Initial estimates for K_h, transmissivity, specific yield, and specific storage were based on field testing or commonly accepted literature values for different materials. Vertical anisotropy in hydraulic conductivity was initially discounted for the alluvium whereby $K_h = K_v$, and set at $K_h = 0.1\ K_v$ for remaining aquifer/aquitard units in both layers. As anisotropy ratios can influence flow paths and effect model results (see Kim et al. 1999), a range of ratios was developed for testing in the model calibration phase.

Further north and further south of the present model domain is strictly laterite terrain that merges into higher ferricrete interfluves, which are designated groundwater divides. The model was not broadened to include these groundwater divides for three reasons: firstly, many more cells would have been needed, thus slowing computational time; secondly, very few wells were situated in these areas and, therefore, the levels of confidence in water level measurements was a lot lower; and thirdly, the lateral extent of the domain was selected to encapsulate flow entering into and out of the alluvial channel system, and it was deemed that a laterite buffer of at least 50 m emplaced around the lateral extent of the alluvial channels would be satisfactory to ensure that no artificial flowpaths were introduced into the channels.

Model calibration

The final calibrated values for model parameters are given in Table 1. Automated inverse modelling using PEST was beneficial in obtaining quick estimates of best-fit parameter values, and to establish degrees of confidence in the field measured values. PEST uses a nonlinear estimation technique known as the Gauss-Marquadt-Levenburg method (Doherty 1994). The calibrated K_h values for hydrofacies units C, E and F were within the range of measured values.

 DOI 10.1007/s10040-005-0470-5

Table 1 Final calibrated values for selected model parameters for the major hydrofacies units

Parameter	Hydrofacies zone	Value	95% Confidence limits	
			Lower limit	Upper limit
K_h m/s (m/d)	A	9.8×10^{-4} (84.67)	8.61×10^{-4} (74.39)	1.24×10^{-3} (107.14)
	B	3.0×10^{-4} (25.92)	1.67×10^{-4} (14.43)	4.09×10^{-4} (35.33)
	C	1.16×10^{-4} (10.02)	0.94×10^{-4} (8.12)	1.78×10^{-4} (15.38)
	D	3×10^{-7} (0.026)	6.1×10^{-8} (0.005)	8.56×10^{-6} (0.74)
	E	3×10^{-7} (0.026)	0.43×10^{-7} (0.004)	8.34×10^{-7} (0.072)
	F	2.5×10^{-6} (0.216)	1.01×10^{-6} (0.086)	1.08×10^{-5} (0.933)
Anisotropy ratio b (K_h/K_v)	A, B	1.0		
	C	5.0		
	D, E	100.0		
	F	25.0		
Specific yield (%)	A, B	0.15		
	C	0.1		
	D, E	0.015		
	F	0.06		

Final K_h values for hydrofacies units A, B, and D were outside of the range of field measurements (by 9, 30 and 50% respectively), however, they were within ranges of laboratory (falling head permeameter and grain size determination) values, and within values calculated in analogous hydrofacies (Klingbeil et al. 1999; Weissmann et al. 2000; Heinz et al. 2003). It should be noted, however, that laboratory values of permeability are often misleading owing to the re-arranging of sediments during both drilling, handling, sample preparation and sample packing phases.

Comparison of observed and predicted heads for the model period (Fig. 7) shows that the patterns match well. Significantly, hydrofacies units A, B, and C within the alluvium had better visual and statistical fits (RMSE of <0.75 m, and IOA of >0.68) than the other clay-rich and indurated units (RMSE of <1.85 m, and IOA of 0.43–0.71).

The water budgets calculated for each of the 40 time steps (20 dry and 20 wet periods) within each of the hydrofacies sub-regions showed a maximum discrepancy of 0.03% for the difference between the total modelled inflow and the total modelled outflow. The balance in the net fluxes is an indicator that the model is conserving mass.

A detailed sensitivity analysis has shown that each hydrofacies zone responds differently to incremental adjustments in particular parameter values (Fig. 8). None of the six hydrofacies returned a Type IV sensitivity to any of the tested parameters. Type IV results invalidate a model by significantly changing model outputs without effecting calibration residuals or acceptance measures (ASTM D 5611-94 1999). Hydrofacies A and F are both sensitive to K_h (Type III), but only after that value is increased or decreased by an order of magnitude. For unit F, which has been affected by weathering and cementation, this order of variability is realistic (considering the low flow rate) and so the degree of uncertainty is warranted. For unit A, however, there is far more confidence in the calibrated K_h value, due to the consistently coarse grain size (<5% fine-grained matrix) associated with the gravel, and a lack of any noticeable sedimentary structures that may impede water flow. For these two reasons it is unlikely that K_h will change from 80 m/day to either 8 m/day or to 800 m/day within that gravelly aquifer unit.

Hydrofacies B, C, D and E were sensitive to changes in specific yield (Type III) from within or from zones directly overlying. Vertical anisotropy was only sensitive for hydrofacies F, which is again warranted due to the variable cementation within that unit.

It should be noted that by defining hydrofacies zones (constrained by GPR) the non-uniqueness of a model shifts from the entire model domain into non-uniqueness associated within each hydrofacies zone. These zones are real and must be adhered to in a modelling sense. Non-uniqueness in each hydrofacies zone remains an ill-posed problem, and through the use of PEST we are presenting one possibility, that may be better determined through sophisticated methods such as entropy, the Monte Carlo method and Bayesian inverse theory (see Sudicky 1986 and Woodbury and Sudicky 1991 for examples).

Model outcomes

The variable trends and magnitudes of shallow groundwater flow within the central plain is illustrated by the patterns of the potentiometric surface elevations as well as maps of velocity vectors and pathlines, calculated from transient simulations (Fig. 9a–d). It is apparent that the alluvial aquifer, and in particular hydrofacies units A and B, is the primary conduit for groundwater, and that the majority of water that enters the central plain in any hydrofacies, flows through to the eastern coastal plain via the semi-confined alluvial delta (A).

Residence times within each hydrofacies have been determined using forward and reverse particle tracking modules. Groundwater that enters the alluvium (hydrofacies A, B or C) takes between 1 and 18 months to exit the flow system. Groundwater within lateritic mixed clay layers (D) have residence times in the order of tens to hundreds of years, while groundwater within ferri-

 DOI 10.1007/s10040-005-0470-5

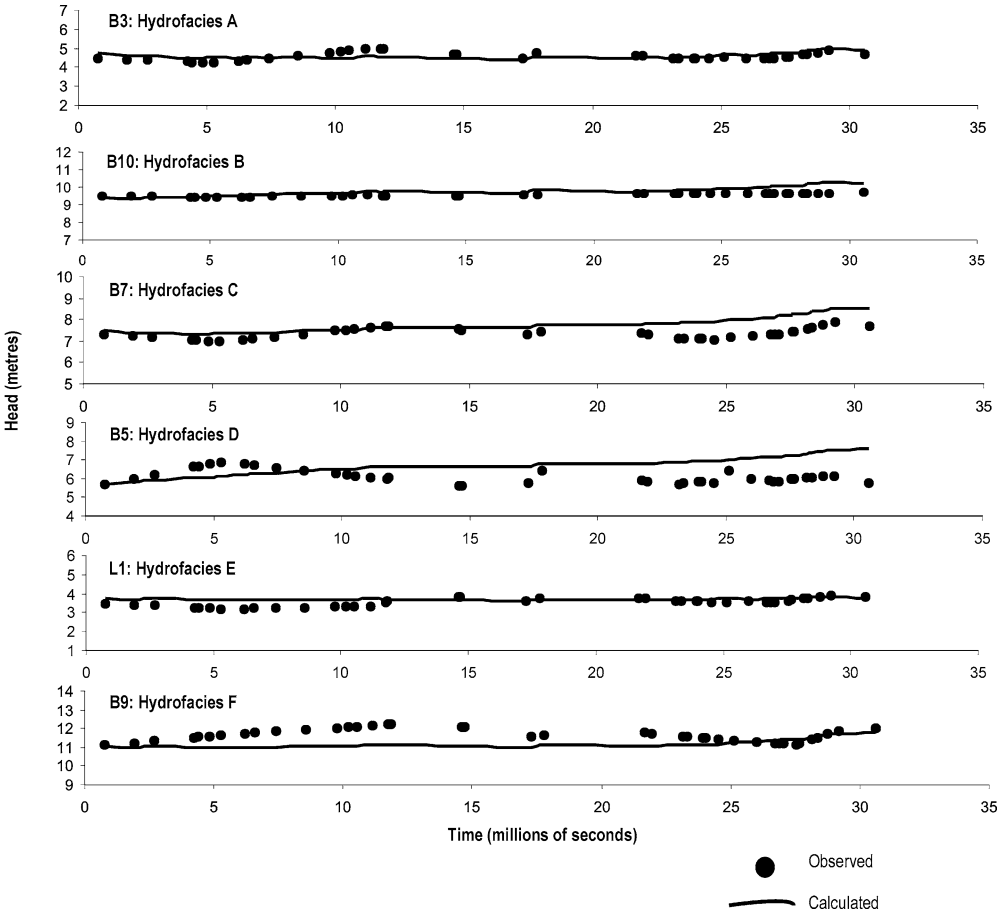

Fig. 7 Calculated versus observed heads (mASL) in six representative wells (one for each hydrofacies unit), for the calibrated transient model period

crete horizons (F) have a maximum residency time of 3 years. Leaky floodplain clays (E) to the east have significant storage capacity and recharge the underlying alluvial delta within one month to several years, depending upon whether the selected anisotropy ratio is set at maximum or minimum.

Discussion

Groundwater flow paths and rates generated in particle tracking modules indicate that fresh groundwater within both alluvial channels and the alluvial delta flows directly into coastal wetlands to the east. These wetlands are also subject to reverse flow (westward) via saline intrusion from the estuary. The moderate to high flow rates of fresh groundwater transmitted out of the alluvial delta (A) ensures that the potential for salt-water intrusion into the alluvial channels (B and C) is low. These higher flow rates also indicate that pollutants which enter alluvial aquifers will readily travel into the coastal wetlands within a period of one year, making remediation deadlines very short. Conversely, pollutants introduced to the water table within hydrofacies units D-F, will be stagnant (assuming they are not too close to alluvial channels) and remediation can be organized correctly and the potential for natural remediation methods can be assessed.

Spatial and temporal variation in groundwater chemical character within each of the hydrofacies supports the outcomes of flow modelling and also indicates that sedimentary heterogeneity is strongly controlling the flow of groundwater. Groundwater hosted within alluvial aquifers is independent of other groundwater bodies in the plain, and slowly evolves from a Na-HCO_3,Cl type in the western, unconfined sections to Na-Cl, HCO_3 to Na-Cl to Na-Cl, SO_4 in the semi-confined coastal reaches to the east of the model domain (Ezzy and Cox 2003). Sulfate reduction, silica equilibrium and limited ion exchange are the dominant chemical processes occurring within the weakly mineralized alluvial groundwaters as they flow down-gradient from west to east at a relatively rapid rate. Conversely, sulfate enrichment, associated with increases in Ca, HCO_3, Fe, and Al in shallow coastal aquifers to the east is attributed to both saline intrusion from the tidal estuary during dry periods, as well as oxidation of sulfide materials in surficial estuarine and marine clays.

In contrast, groundwater within the laterite is strongly enriched in both Fe and Mg (3 orders of magnitude greater than alluvial groundwater), and contains very little HCO_3 (two orders of magnitude less). The relative Mg-enrichment

 DOI 10.1007/s10040-005-0470-5

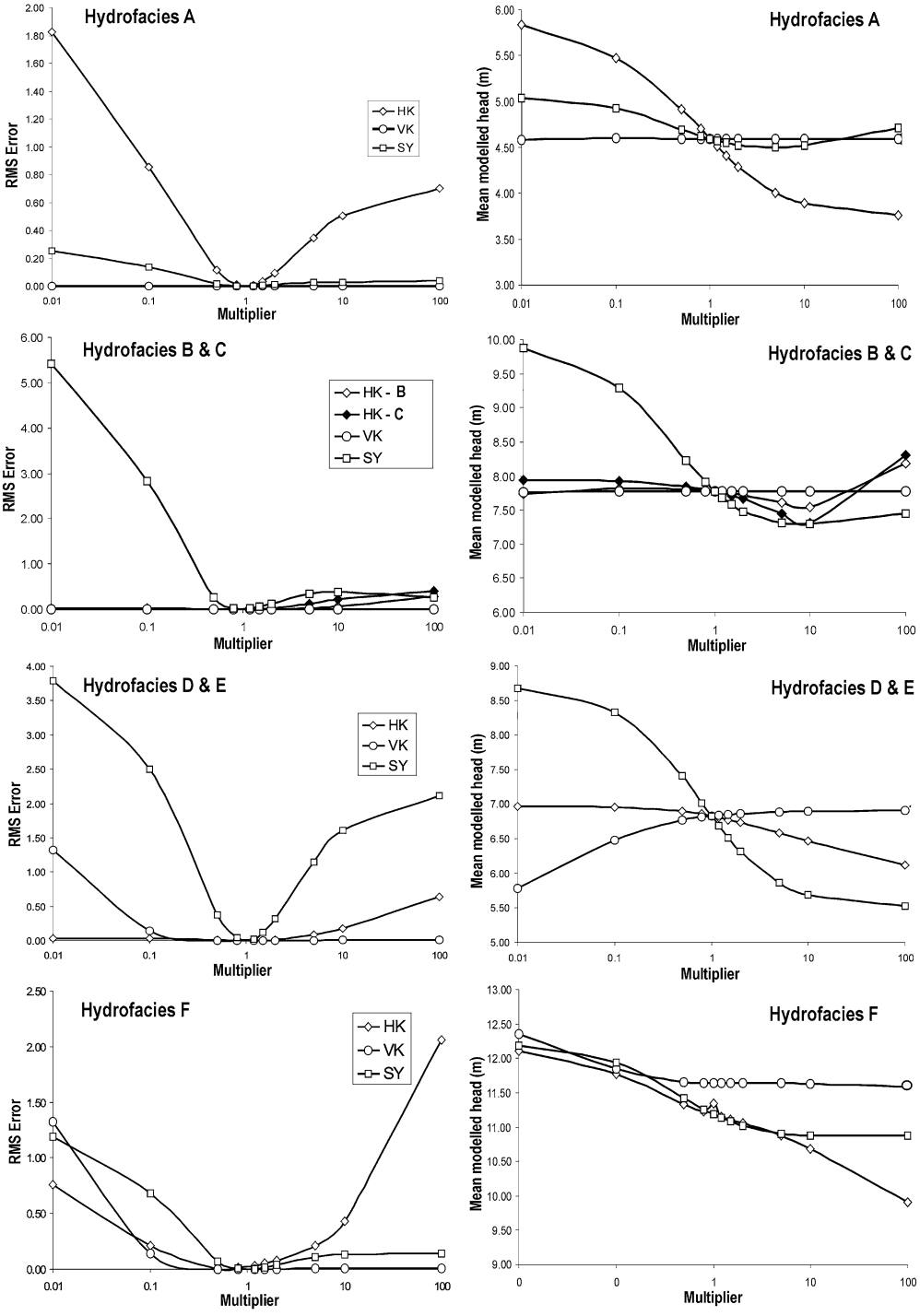

Fig. 8 Statistical plots showing results of the sensitivity analysis conducted on calibrated parameters of K_h, K_v, and specific yield for each of the major hydrofacies units. Plots on the left compare sensitivity multipliers (logarithmic scale) with the calculated RMSE for each of the parameters, while plots on the right compare the same sensitivity multipliers with mean modelled head

is attributed to sediment-water interactions between fresh Na-Cl groundwater and smectite (a common clay phase within the laterite). Higher levels of Fe (>30 mg/L) are regularly encountered in those weathered bedrock groundwaters due to migration through coarser palaeochannel sand layers that are rich in secondary hematite-cement.

Cross-checking the range of hydraulic parameters determined from field and laboratory testing, with the automated inverse parameter estimation program PEST helped to assess the degree of heterogeneity between hydrofacies units as well as within each unit, and also assess the reliability of the determined parameters. An example of this reliability is evident for units B and C within the allu-

 DOI 10.1007/s10040-005-0470-5

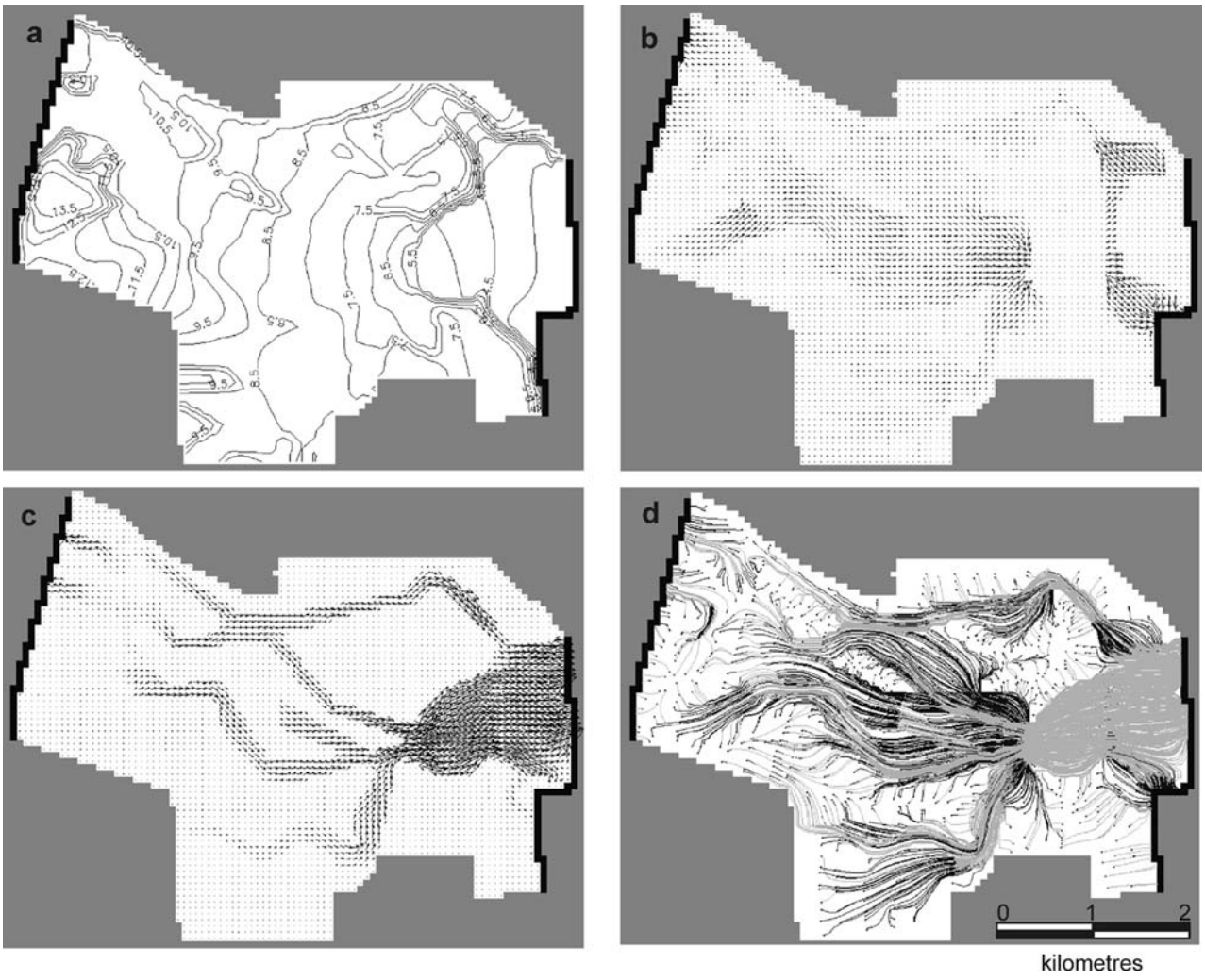

Fig. 9 Maps of various groundwater flow features calculated at the end of the transient simulation: **a** contours of the calculated heads (m) within the model domain; **b** calculated velocity vectors for layer 1; **c** calculated velocity vectors for layer 2, and; **d** forward tracking of randomly scattered particles after a 200 year period. Black pathlines represent flow in layer 1, while grey lines represent flow in layer 2. Black cells along the west and east boundaries of model domain represent constant head cells

vial channels, with mean measured K_h values of 13.38 and 9.28 m/day, respectively. Best-fit values for these units were 25.92 m/day (33% greater than maximum measured value) for unit B, and 10.02 m/day (9% greater than mean measured value) for unit C. The variability between measured and best-fit values for unit B is attributed to lateral grain size (medium- and coarse-grained sand) variations. At a macroscopic scale these subtle internal variations within sand-prone hydrofacies have little effect on subsequent particle tracking experiments when compared to changes in large-scale aquifer geometries, and changes in permeability between facies. However, if higher resolution was required for a site-specific (tens of metres) contamination problem within the alluvium, the calibrated macroscopic flow model would provide essential information on groundwater flowpaths, rates, and parameter ranges. This information could then be applied to a more detailed flow model, that incorporates meso-scale or micro-scale heterogeneity obtained from a new tightly-spaced GPR grid (e.g. Bevan et al. 2003). Mathematical processing (e.g. correlation structures) of the original GPR data-set in combination with tracer tests may also provide a much more detailed account of the hydraulic parameters within individual hydrofacies units, enabling finer-scale modelling and predictions of flowpaths.

The major limitation to the approach is a lack of sedimentary detail from 3 to 9 m depth within the laterite profile and floodplain, due to rapid attenuation of the GPR signal in this material. This lack of data results in inadequate characterisation of aquifer architecture. Statistical and visual comparisons of simulated versus observed heads within observation wells, contained much higher rates of systematic error for hydrofacies D, E and F compared to hydrofacies A, B and C. This can be attributed to the fact that unmodelled heterogeneity causes error in the simulated heads (Anderson and Woessner 1992).

 DOI 10.1007/s10040-005-0470-5

Conclusions

There is significant macroscopic heterogeneity between fine-grained lateritic mixed clay layers, floodplain clays, iron-cemented ferricrete horizons, and permeable sand-rich alluvial aquifers in this low-lying coastal alluvial plain. This high variety of aquifer material has created a complex subsurface arrangement of permeability pathways. The interconnection of narrow alluvial channels feeding into a deeper alluvial delta has provided a significant conduit for shallow groundwater flow. Application of various geological techniques in this setting has confirmed that GPR profiles provide information between wells enabling accurate definition of alluvial channel boundaries and determination of the high degree of connectedness within the channels themselves. Finite-difference groundwater modelling and particle tracking analysis has clearly demonstrated that the macroscopic heterogeneity both within-facies and between, has marked impacts on groundwater pathways and especially groundwater travel times in this plain. The variability between a maximum residence time of 18 months for groundwater within the alluvium, compared to hundreds of years for groundwater within the mixed clay layers of the laterite, clearly demonstrates the importance of accurately defining the spatial distribution of the various aquifer materials in a groundwater flow investigation. The role of the alluvial delta in discharging the bulk of fresh groundwater from the central plain into the coastal and estuarine aquifers to the east, is certainly critical in preventing saline intrusion from encroaching further west.

Acknowledgements The authors express their gratitude to CSIRO Mineral Exploration and Mining Division for use of their RAMAC GPR unit, Dr. David Noon (University of Queenland) for GPR technical advice, and Lensworth (particularly Dr. Ron Black, and Peter Gust) for research funding and technical support. The authors are indebted to Dr. Daniel Lack for invaluable advice regarding sensitivity analysis and assistance in compiling the statistical code.

References

Anderson MP (1989) Hydrogeological facies models to delineate large-scale spatial trends in glacial and glacio-fluvial sediments. GSA Bull 101:501–511

Anderson MP, Aiken JS, Webb EK, Mickelson DM (1999) Sedimentology and hydrogeology of two braided stream deposits. Sed Geol 129:187–199

Anderson MP, Woessner WW (1992) Applied groundwater modeling: simulation of flow and advective transport. Academic Press, Toronto, Ontario, Canada

Asprion U, Aigner T (1997) Aquifer architecture analysis using ground-penetrating radar: Triassic and Quaternary examples (S. Germany). Envir Geol 31:66–75

Asprion U, Aigner T (1999) Towards realistic aquifer models: three-dimensional georadar surveys of Quaternary gravel deltas (Singen Basin, SW Germany). Sed Geol 129:281–297

ASTM D 5611-94 (1999) Standard guide for conducting a sensitivity analysis for a ground-water flow model application, American Society for Testing and Materials, 5 pp

Beres M, Huggenberger P, Green AG, Horstmeyer H (1999) Using two- and three-dimensional georadar methods to characterise glaciofluvial architecture. Sed Geol 129:1–24

Bersezio R, Bini A, Guidici M (1999) Effects of sedimentary heterogeneity on groundwater flow in a Quaternary pro-glacial delta environment: joining facies analysis and numerical modelling. Sed Geol 129:327–344

Best JL, Ashworth PJ, Bristow CM, Roden J (2003) Three-dimensional sedimentary architecture of a large, mid-channel sand braid bar, Jamuna River, Bangladesh. J Sed Res 73:516–530

Bevan MJ, Endres AL, Rudolph DL, Parkin G (2003) The non-invasive characterization of pumping-induced dewatering using ground penetrating radar. J Hydrol 281:55–69

Bridge JS, Alexander J, Collier REL, Gawthorpe RL, Jarvis J (1995) Ground-penetrating radar and coring used to study the large-scale structure of point-bar deposits in three dimensions. Sedimentology 42:839–852

Bridge JS, Collier REL, Alexander J (1998) Large-scale structure of Calamus River deposits (Nebranska, USA) revealed using ground-penetrating radar. Sedimentology 45:977–986

Bristow CS, Chroston PN, Bailey SD (2000) The structure and development of foredunes on a locally prograding coast: insights from ground-penetrating radar surveys, Norfolk, UK. Sedimentology 47:923–944

Carle SF, Labolle EM, Weissmann GS, Van Brocklin D, Fogg GE (1998) Conditional simulation of hydrofacies architecture: a transition probability/Markov approach. In: Fraser GS, Davis JM (eds) Hydrogeologic models of sedimentary aquifers, vol 1: concepts in hydrogeology and environmental geology no 1. SEPM, Oklahoma, USA, pp 147–170

Chiang WH, Kinzelbach W (1998) Processing Modflow Version 5.0 Operation Manual Hamburg, Heidelberg, Germany, Scientific Software Group

Cooper HH, Bredehoeft JD, Papadopulos IS (1967) Response of a finite-diameter well to an instantaneous charge of water. Water Resour Res 3:263–269

Cooper HH, Jacob CE (1946) A generalized graphical method for evaluating formation constants and summarizing well field history. Am Geophys Union Trans 27:526–534

Cranfield LC (1984) Stratigraphic drilling data—Ipswich, Brisbane and Gympie 1:250, 000 Sheet areas—1972 to 1976. Geological Survey of Queensland, Brisbane

Doherty J (1994) PEST model-independent parameter estimation. Watermark Computing, Corinda, Australia, 122 pp

Dominic DF, Ritzi RW, Reboulet EC, Zimmer AC (1998) Geostatistical analysis of facies distributions: elements of a quantitative facies model. In: Fraser GS, Davis JM (eds) Hydrogeologic models of sedimentary aquifers, vol 1: concepts in hydrogeology and environmental geology no 1. SEPM, Oklahoma, USA, pp 137–146

Ezzy TR, Cox ME (2003) Implications of land-use changes on groundwater within shallow coastal plain aquifers, Bells Creek catchment, southeast Queensland, Australia. In: Lopez-Geta JA, de la Orden JA, de Dios Gomez J, Ramos G, Mejias M, Rodriguez L (eds) Coastal aquifers intrusion technology: Mediterranean countries, vol 1: hidrogeologia Y aguas subterraneas no 8. Instituto Geologico Y Minero de Espana, Alicante, Spain, pp 439–444

Ezzy TR, Cox ME, Brooke B (2002) The influence of stratigraphy on the occurrence and composition of groundwater within a coastal valley-fill: Meldale, southeastern Queensland. In: "Balancing the Groundwater Budget" CD of Proceedings, 7th IAH National Groundwater Conference, Darwin, 12–17 May, 2002, 6 pp

Fogg GE, Noyes CD, Carle SF (1998) Geologically based model of heterogeneous hydraulic conductivity in an alluvial setting. Hydrogeol J 6:131–143

Galloway WE, Sharp JM (1998a) Characterising aquifer heterogeneity within terrigenous clastic depositional systems. In: Fraser GS, Davis JM (eds) Hydrogeologic models of sedimentary aquifers, vol 1: concepts in hydrogeology and environmental geology no 1. SEPM, Oklahoma, USA, pp 85–90

 DOI 10.1007/s10040-005-0470-5

Galloway WE, Sharp JM (1998b) Hydrogeology and characterisation of fluvial aquifer systems. In: Fraser GS, Davis JM (eds) Hydrogeologic models of sedimentary aquifers, vol 1: concepts in hydrogeology and environmental geology no 1. SEPM, Oklahoma, USA, pp 91–106

Grant JA, Brooks MJ, Taylor BE (1998) New constraints on the evolution of the Carolina Bays from ground-penetrating radar. Geomorphology 22:325–345

Haitjema H, Kelson V, de Lange W (2001) Selecting MODFLOW cell sizes for accurate flow fields. Ground Water 39:931–938

Harari Z (1996) Ground-penetrating radar (GPR) for imaging stratigraphic features and groundwater in sand dunes. J Appl Geophys 36:43–52

Heinz J, Kleineidam S, Teutsch G, Aigner T (2003) Heterogeneity patterns of Quaternary glaciofluvial gravel bodies (SW Germany): application to hydrogeology. Sed Geol 158:1–23

Huggenberger P, Aigner T (1999) Introduction to the special issue on aquifer sedimentology: problems, perspectives and modern approaches. Sed Geol 129:179–186

Hvorslev MJ (1951) Time lag and soil permeability in ground-water observations, US Army Corps of Engineers Waterways Experiment Station. Bulletin no 36, 50 p

Kim K, Anderson MP, Bowser CJ (1999) Model calibration with multiple targets: a case study. Ground Water 37:345–351

Klingbeil R, Kleineidam S, Asprion U, Aigner T, Teutsch G (1999) Relating lithofacies to hydrofacies: outcrop-based hydrogeological characterisation of Quaternary gravel deposits. Sed Geol 129:299–310

Koltermann CE, Gorelick SM (1996) Heterogeneity in sedimentary deposits: a review of structure-imitating, process-imitating, and descriptive approaches. Water Resour Res 32:2617–2658

Leclerc RF, Hickin EJ (1997) The internal structure of scrolled floodplain deposits based on ground-penetrating radar, North Thompson River, British Columbia. Geomorphology 21:17–38

Martin JE, O'Flynn ML, Willmott WF (1978) Industrial rock and mineral resources: Nambour and Caloundra 1:100,000 sheet areas, Department of Mines, Geological Society of Queensland, Record 1978/16

McDonald MG, Harbaugh AW (1988) A modular three-dimensional finite difference groundwater flow model, USGS techniques of water-resources investigations, Book 6, Chap. A1: 586 pp

McKellar JL (1993) Stratigraphic relationships in the Nambour Basin, southeastern Queensland. In: Beetson JW (ed) Queensland geology. Department of Minerals and Energy, Brisbane, pp 1–17

Middlemis H (2001) Murray-Darling Basin Commission: Groundwater flow modelling guideline. Aquaterra Consultancy Pty Ltd, South Perth, Western Australia, 133 pp

Miller RB, Castle JW, Temples TJ (2000) Deterministic and stochastic modeling of aquifer stratigraphy, south Carolina. Ground Water 38:284–295

Neal A, Richards J, Pye K (2002) Structure and development of shelf cheniers in Essex, southeast England, investigated using high-frequency ground-penetrating radar. Marine Geol 185:435–469

Neal A, Roberts CL (2000) Applications of ground-penetrating radar (GPR) to sedimentological, geomorphological and geoarchaeological studies in coastal environments. In: Pye K, Allen JRL (eds) Coastal and estuarine environments: sedimentology, geomorphology and geoarchaeology, vol 175. Geological Society, London, Special Publications, pp 139–171

Neuman SP (1972) Theory of flow in unconfined aquifers considering delayed response of the watertable. Water Resour Res 8:1031–1045

Nobes DC, Ferguson RJ, Brierley GJ (2001) Ground-penetrating radar and sedimentological analysis of Holocene floodplains: insight from the Tuross valley, New South Wales. Aust J Earth Sci 48:347–355

O'Rourke A (2002) The sedimentary framework and aquifer characteristics of the Bells Creek plain, Australia, determined using Ground Penetrating Radar. Unpublished BSc (hons), Queensland University of Technology

Poeter E, Gaylord DR (1990) Influence of aquifer heterogeneity on contaminant transport at the Hanford Site. Ground Water 32(3):439–447

Pollock DW (1989) Documentation of computer programs to compute and display pathlines using results from the U.S. Geological Survey modular three-dimensional finite-difference groundwater model. USGS Open-File Report 89-381: 188 pp

Stanford SD, Ashley GM (1998) Using three-dimensional geologic models to map glacial aquifer systems: an example from New Jersey. In: Fraser GS, Davis JM (eds) Hydrogeologic models of sedimentary aquifers, vol 1: concepts in hydrogeology and environmental geology no 1. SEPM, Oklahoma, USA, pp 69–84

Sudicky EA (1986) A natural gradient experiment on solute transport in a sand aquifer. Spatial variability of hydraulic conductivity and its role in the dispersion process. Water Resour Res 22:2069–2082

Theis CV (1935) The relation between the lowering of the piezometric surface and the rate and duration of discharge of a well using groundwater storage. Trans Am Geophys Union 16:519–524

van Overmeeren RA (1998) Radar facies of unconsolidated sediments in The Netherlands: A radar stratigraphy interpretation method for hydrogeology. J Appl Geophys 40:1–18

Vandenberghe J, van Overmeeren RA (1999) Ground penetrating radar images of selected fluvial deposits in the Netherlands. Sed Geol 128:245–270

Webb EK, Davis JM (1998) Simulation of the spatial heterogeneity of geologic properties: an overview. In: Fraser GS, Davis JM (eds) Hydrogeologic models of sedimentary aquifers, vol 1: concepts in hydrogeology and environmental geology no 1. SEPM, Oklahoma, USA, pp 1–24

Weissmann GS, Labolle EM, Fogg GE (2000) Modeling environmental tracer-based groundwater ages in heterogeneous aquifers. In: Bentley LR, Sykes JF, Brebbia CA, Gray WG, Pinder GF (eds) Computational methods in water resources. A.A. Balkema, Calgary, Alberta, Canada, 25–29 June, pp 805–811

Willmott CJ (1981) On the validation of models. Phys Geog 2:184–194

Willmott WF, Stevens NC (1988) Rocks and landscapes of the Sunshine Coast Brisbane, Geological Society of Australia

Woodbury AD, Sudicky EA (1991) The Geostatistical characteristics of the Borden aquifer. Water Resour Res 27:533–546

 DOI 10.1007/s10040-005-0470-5